Synthesis, Reactivity, X-ray characterization and Docking studies of N^7/N^9-(2-pyrimidyl)-Adenine derivatives

Daniel Martínez[a], Adriá Pérez[a], Santiago Cañellas[a], Ivan Silió[a], Aida Lancho[a], Angel García-Raso*[a], Joan J. Fiol[a], Angel Terrón[a], Miquel Barceló-Oliver[a], Joaquín Ortega-Castro[a], Elies Molins[b], and Antonio Frontera*[a]

[a]*Departament de Química, Universitat de les Illes Balears, Crta. de Valldemossa km 7.5, 07122 Palma de Mallorca (Baleares), Spain.*

[b]*Institut de Ciència de Materials de Barcelona (CSIC), Campus UAB, 08193 Bellaterra, Spain*

*Corresponding authors: (A. Frontera) E-mail: toni.frontera@uib.es; (A. García-Raso) E-mail: angel.garcia-raso@uib.es; FAX: +34 971173426

"In memoriam of Professor Juan Manuel Salas Peregrín and his contribution to the research on bioinorganic chemistry in Spain"

Abstract

The reaction of adenine with 2-chloropyrimidine yields as a major product the unexpected N^7-(2-pyrimidyl)-adenine (**1**) and as a minor one N^9-(2-pyrimidyl)-adenine (**2**). Both compounds have been characterized by X-ray diffraction analysis. Moreover, we report the formation of a 1:1 co-crystal (**3**) composed by compound (**1**) and adenine that was formed serendipitously during the synthesis of (**1**). Unexpectedly, the treatment of (**1**) with Brönsted acids like HCl or HNO_3 causes the opening of the imidazole ring of the N^7-substituted adenine, yielding N^5-(pyrimidin-2-yl)pyrimidine-4,5,6-triamine (**4-7**) which we have X-ray characterized in its neutral, (**4**), monoprotonated [nitrate salt (**6**)] and diprotonated forms [hydrochloride salt (**5**) and, also, a tetrachlorozincate salt (**7**)]. Finally, we have used compound (**5**) as ligand to synthesize and X-ray characterize its complexes with Ir(III) and Ag(I) (compounds (**8**) and (**9**), respectively), where the latter is a 2D coordination polymer and the former is a discrete mononuclear complex. We have studied the supramolecular assemblies formed in the solid state by using density functional theory (DFT) calculations. Finally, DNA-docking studies of several compounds have been carried out in order to analyze their ability to interact with the DNA.

Keywords: Adenine complexes; Ir(III) complexes; Ag(I) complexes; DFT calculations; Supramolecular chemistry; Docking studies

Introduction

Natural purine nucleosides substituted in N^9 have been studied for many years due to their biological activity, in particular as antiviral and anti-proliferative compounds [1–3]. N^7-nucleoside derivatives are less commonly studied [4–7], and usually limited to N^7/N^9-glycosyl transfer processes [8]. The standard method to synthesize N^9-alkyladenines is the alkylation of the nucleobase in the presence of a base [9–11]. The regioselectivity of the alkylation reaction depends on the experimental conditions and the substitution of the purine base. In general, the N^7 and N^3 regioisomers [12–15] are obtained as side products where the major product is the N^9-regioisomer. Predicting the site of alkylation is very difficult in protected or modified adenine [16,17] and in some particular cases the N^7-isomer is the major product. For example, it has been shown that the alkylation of N^6-[(N,N-dimethylamino)methylene]adenine with certain alkylating reagents leads selectively to the N^7-substituted derivatives [18].

We have previously reported [19–21] the synthesis and X-ray characterization of N^6-substituted adenines (including N^6-aminoacid/peptide substitution) since they are interesting substrates due to their cytokinin activity [22]. In this new investigation, we report the synthesis, characterization and X-ray crystal structures of several adenine derivatives, salts and complexes. The neutral compounds are N^7-(2-pyrimidyl)-adenine (**1**), N^9-(2-pyrimidyl)-adenine (**2**), [adenine·(**1**)] cocrystal (**3**) and N^5-(pyrimidin-2-yl)pyrimidine-4,5,6-triamine (**4**) (also denoted as L) which is formed upon addition of Brönsted acid to (**1**). The salts and complexes are $(H_2L)(Cl)_2$ (**5**), $(HL)(NO_3)$ (**6**), $(H_2L)(ZnCl_4)$ (**7**), $[Ir(L)(DMSO)(Cl)_3]$ (**8**) and $\{[Ag_2L(NO_3)_2]\cdot H_2O\}_n$ (**9**). In the Ir(III) complex the ligand is in its zwitterionic form with a protonated pyrimidinic ring and the deprotonated amino group yielding a four member metallocycle. The unexpected formation of (**4**) from (**1**) (see Scheme 1) can be envisaged as a convenient route for the synthesis of (2-pyrimidyl)-(5-pyrimidyl)amines that have not been investigated in the literature, neither as ligands for coordination chemistry nor for biological activity. The theoretical study has been divided into two different parts: (i) the analysis of the supramolecular assemblies in the solid state taking advantage of DFT calculations and theoretical models and (ii) the study of the potential biological importance of the synthesized organic ligands and Ir(III) complex by exploring their interaction with DNA using molecular docking calculations.

Insert here Scheme 1

Experimental

Materials and measurements

Chemicals and solvents were purchased from commercial sources (Sigma-Aldrich) and were used as received. FT-IR spectra in the solid state (KBr pellets) were measured in the 4000-400 cm^{-1} range on a Bruker Tensor 27 spectrometer. ^{1}H and ^{13}C NMR spectra were recorded at room temperature on a Bruker AMX 300 or a Bruker Avance 500 Ultrashield apparatus operating at 500 MHz. Proton and carbon chemical shifts in dimethyl sulfoxide (DMSO-d_6) or methanol (methanol-d_4) solutions were referenced to the corresponding DMSO-d_6 [^{1}H NMR, δ(DMSO) = 2.50; ^{13}C NMR δ(DMSO) = 39.5 ppm] or methanol-d_4 [^{1}H NMR, δ(methanol) = 3.34; ^{13}C NMR δ(methanol) = 49.9 ppm]. Electrospray ionization-high resolution mass spectra (ESI-HRMS) were made in a Qexactive-Thermo Scientific apparatus, with an Orbitrap analyser (samples were dissolved in DMSO for the first dilution and methanol in the second dilution). Thermogravimetric data in the temperature range from 30 to 800ºC were recorded in a flowing oxygen atmosphere (heating range 5 ºC/min) on a PE TGA-2 thermobalance. In Supplementary material, conditions for DNA cleavage studies have been included, although the compounds reported in this paper have not shown any cleavage capability, even at concentration of 1 mM, after 24 h incubation at 37 ºC in the dark.

Preparation of the compounds

Synthesis of N^7-(2-pyrimidyl)-adenine (1). 5.2 mmol of adenine (700 mg), 240 mg of NaH (60%) and 10 mL of anhydrous DMF were mixed during 30 min in a round bottom flask at 0ºC under argon atmosphere. Then, 5.2 mmol of 2-chloropyrimidine (600 mg) were added to the mixture that was heated at 90 ºC for 3 h. Afterwards, the solution was allowed to reach room temperature and maintained unperturbed. A yellow precipitate that corresponds to compound (**1**) was formed, which was filtered off, washed with water and acetone and allowed to dry at room temperature (70%). M.p. 230 – 235 ºC(d). IR (KBr, cm^{-1}): 3595m, 3314m, 3170m, 3125m, 1797w, 1664s, 1574s, 1550s, 1483s, 1432s, 1395m, 1349m, 1319s, 1267m, 1242m, 1198m, 1197m, 1111m, 822m, 789m,

664m, 642m, 622m, 603m, 590m. ^{1}H NMR (ppm) (300 MHz; DMSO-d_6): 9.24s [1H, C8-H], 8.97d [2H, *J* = 4.8 Hz, C4a-H and C6a-H], 8.28s [1H, C2-H], 7.58t [1H, *J* = 4.8Hz, C5a-H]. ^{13}C NMR (ppm) (75 MHz; DMSO-d_6): 162.3 [C4], 160.6 [C4a and C6a], 155.1 [C2a], 154.9 [C2], 153.4 [C6], 145.7 [C8], 120.6 [C5a], 109.8 [C5]. ESI-HRMS: [**1** + Na]$^{+}$, $C_9H_7N_7Na$: exp: 236.0645; cald: 236.0661.

Synthesis of N^{9}-(2-pyrimidyl)-adenine (2). During the synthesis of (**1**) (see above), after the filtration of the yellow precipitate (**1**), the resulting liquid (DMF solution) was evaporated and the solid resulted to be a 1:1 mixture of (**1**) and (**2**), as determined by ^{1}H-NMR. Isomers **1** and **2** were separated by preparative HPLC purification in a Chiralpak IC column and MeOH (0.1% diethylamine) as eluent (see ESI for more information). Alternatively, if the DMF solution is kept unperturbed (instead of evaporated) during several months, a few octahedral crystals of (**2**) appear at the bottom of the flask suitable for X-ray diffraction analysis. IR (KBr, cm^{-1}): 3596s, 3316vs, 3174s, 3125vs, 2926m, 2854m, 1796w, 1644vs, 1575s, 1551s, 1484vs, 1431vs, 1401s, 1385m, 1349vs, 1286m, 1243m, 1199m, 1179s, 1111m, 1077w, 1036w, 1004w, 989w, 903w, 823m,790s, 761w, 724w, 667s,643s, 623m, 604s, 591s, 564w, 514w, 477w, 458w. ^{1}H NMR (ppm) (500 MHz; methanol-d_4): 8.99s [1H, C8-H], 8.96d [2H, *J* = 4.8 Hz, C4a-H and C6a-H], 8.39s [1H, C2-H], 7.55t [1H, *J* = 4.8 Hz, C5a-H]. ^{13}C NMR (ppm) (125 MHz; methanol-d_4): 160.5 [C4a and C6a], 158.0 [C4], 156.1 [C2], 155.0 [C2a], 150.0 [C6], 141.2 [C8], 121.7 [C5], 121.3 [C5a]. ESI-HRMS: [**2** + Na]$^{+}$, $C_9H_7N_7Na$: exp: 236.0650; cald: 236.0661; [(**2**)$_2$ + Na]$^{+}$, $(C_9H_7N_7)_2Na$: exp: 449.1406; cald: 449.1418.

Synthesis of cocrystal [adenine:1] (3): In one of the attempts to synthesize compound (**1**), few crystals of compound (**3**) were serendipitously obtained that correspond to a co-crystal of compound (**1**) with the starting product, adenine. It should be mentioned that we have not been able to reproduce the synthesis of (**3**), which has been only characterized by X-ray diffraction. It is included here only for the sake of scientific knowledge.

N^{5}-(pyrimidin-2-yl)pyrimidine-4,5,6-triamine (4): Compound (**1**) (60.6 mg, 0.284 mmol) was dissolved in aqueous HCl (0.5 M, 7.67 mL) and heated up to 90 ºC for 1 hour. Then, the crude mixture was treated with NaOH (2 M) until basic pH, appearing a white precipitate. The product was filtered, washed with cold water (1 x 3 mL) and dried overnight in the vacuum oven, giving rise to the desired product (**4**) as a white

solid in quantitative yield (98%). In order to obtain single X-ray crystal quality, 20 mg of (**4**) were dissolved in MeOH and heated up to 40 ^{o}C in an oil bath. The filtered solution was let to cool down slowly in the oil bath to room temperature, rendering white crystals suitable for the single X-ray crystal analysis. IR (KBr, cm^{-1}): 3442m, 3357s, 3193m, 3105m, 2922w, 2853w, 1658m, 1624s, 1593s, 1565s, 1487s, 1463s, 1444s, 1385w, 1329w, 1258w, 1185w, 1012w, 814w, 763w, 643w. ^{1}H NMR (ppm) (300 MHz; DMSO-d_6): 8.30d [2H, *J* = 4.8 Hz, C4a-H and C6a-H], 7.87s [1H, N7-H], 7.74s [1H, C2-H], 6.69t [1H, *J* = 4.8 Hz, C5a-H], 5.77s [4H, N6-H and N9-H] ^{13}C NMR (ppm) (75 MHz; DMSO-d_6): 161.8 [C2a], 160,7 [C6, C4], 158.5 [C6a and C4a], 155.5 [C2], 111.9 [C5a], 97.5 [C5]. ESI-HRMS: [**4** + H]$^{+}$ $C_8H_{10}N_7$: exp 204.0984; cald: 204.0992.

Synthesis of $(H_2L)(Cl)_2$ (5): The synthetic protocol is identical to that explained above for compound (**4**). In this case the clear solution is not neutralized with NaOH and, instead, it is allowed to slowly evaporate at room temperature, crystals of (**5**) appeared at the bottom of the flask after several weeks. IR (KBr, cm^{-1}): 3295m, 3127m, 1649s, 1603s, 1571m, 1551s, 1460m, 1448m, 1419w, 1395w, 1374w, 1340m, 1319w, 1271w, 1253w, 1212w, 1202w, 796w, 776w, 555w ^{1}H NMR (ppm) (300 MHz; DMSO-d_6): 8.91s [1H, N7-H], 8.52d [2H, *J* = 5.1 Hz, C4a-H and C6a-H], 8.24s [1H, C2-H], 7.75s [4H, N6-H and N9-H], 6.96t [1H, *J* = 5.1 Hz, C5a-H]. ^{13}C NMR (ppm) (75 MHz; DMSO-d_6): 158.6 [C2a], 158.2 [C6a and C4a], 156.9 [C4, C6], 148.1 [C2], 112.6 [C5a], 93.3 [C5]. ESI-HRMS: [**4** + H]$^{+}$ $C_8H_{10}N_7$: exp 204.0988; cald: 204.0992.

Synthesis of $(HL)(NO_3)$ (6): A suspension of 2.4 mmol (0.10 g) of (**1**) in 50 mL of HNO_3 0.1 M was refluxed during 3 h (a clear solution is obtained after 15 min). The resulting solution is allowed to reach room temperature and filtered. The slow evaporation of the clear solution at room temperature yields 0.06 g (63%) of white crystals, suitable for X-Ray diffraction, after 4 weeks. IR (KBr, cm^{-1}): 3365w, 3292w, 3177w, 3126w, 3028w, 3009w, 2924w, 2854w, 2799w, 1654s, 1618m, 1565vw, 1500vw, 1453vw, 1440w, 1384vs, 1323m, 1279w, 1255vw, 1205vw, 996vw, 802vw, 777vw, 648vw, 630vw. ^{1}H NMR (ppm) (300 MHz; DMSO-d_6): 8.44d [2H, *J* = 4.9 Hz, C4a-H and C6a-H], 8.19s [1H, C2-H], 7.58s [4H, N6-H and N9-H], 6.87t [1H, *J* = 4.9 Hz, C5a-H]. ^{13}C NMR (ppm) (75 MHz; DMSO-d_6): 158.6 [C2a], 158.3 [C6a and C4a], 156.9 [C4, C6], 148.5 [C2], 112.6 [C5a], 93.3 [C5]. ESI-HRMS: [**4** + H]$^{+}$ $C_8H_{10}N_7$: exp 204.0986; cald: 204.0992.

Synthesis of (H_2L)($ZnCl_4$) (7): A suspension of 0.5 mmol (100 mg) of (**1**) and 1 mmol (140 mg) of $ZnCl_2$ in 20 mL of HCl 0.45 M was refluxed during 4h. Then it was filtered and allowed to reach room temperature. The slow evaporation of the clear solution yields suitable crystals (35%) for X-ray analysis after 8 weeks. IR (KBr, cm^{-1}): 3390m, 3247m, 1658s, 1620s, 1519m, 1500m, 1424m, 1351m, 1276m, 994w, 802w, 772w, 750w, 468w ^{1}H NMR (ppm) (300 MHz; DMSO-d_6): 8.38d [2H, *J* = 5.1 Hz, C4a-H and C6a-H], 8.22s [1H, N7-H], 8.18s [1H, C2-H], 7.55s [4H, N6-H and N9-H], 6.81t [1H, *J* = 5.1 Hz, C5a-H]. ^{13}C NMR (ppm) (75 MHz; DMSO-d_6): 158.6 [C2a], 158.2 [C6a and C4a], 156.9 [C4, C6], 148.3 [C2], 112.7 [C5a], 93.4 [C5]. ESI-HRMS: [**4** + H]$^+$ $C_8H_{10}N_7$: exp 204.0986; cald: 204.0992.

Synthesis of [Ir(L)(DMSO-*κ*S)Cl_3] (8): A solution of 0.0375 mmol (10.35 mg) of compound **5** in 2 mL of water was added to a solution of 0.075 mmol (48.47 mg) of $[IrCl_4(DMSO)_2]\cdot DMSO_2H$ in 2 mL of H_2O and heated at 90ºC without stirring during 6 h. The resulting solution was allowed to reach room temperature and maintained unperturbed. After two days at room temperature, the solution was cooled at 4ºC and a few orange needles, suitable for X Ray diffraction, that correspond to Ir(III) complex (**8**), were obtained after three days. IR(KBr, cm^{-1}): 3453s, 3414vs, 3287vs, 3250s, 3197s, 3001w, 2917w, 2854w, 2767w, 2722w, 2640w, 1666vs, 1632s, 1596s, 1580s, 1520s, 1520m, 1480m, 1453m, 1415m, 1397w, 1382w, 1344vw, 1315m, 1286vw, 1189vw, 1099s, 1024m, 982vw, 916vw, 801w, 780m, 752vw, 735vw, 695m, 666m, 648m, 581w, 562m, 513w, 451w, 437w, 421w. ^{1}H NMR (ppm) (300 MHz; DMSO-d_6) tentative assignment: 9.19s[1H, N-H], 9.03dd [1H, *J* = 6.0 and 1.2 Hz, C4a-H], 8.36br m [1H, C6a-H], 8.16s [1H, C2-H],7.53s [4H, N6-H and N9-H] 6.92br t [1H, *J* = 6.0 Hz, C5a]. ESI-HRMS: [**8**(Ir^{II})-H + Cl]$^-$ $C_{10}H_{15}ON_7{}^{35}Cl_4{}^{191}Ir{}^{32}S$: exp 611.9404; cald: 611.9419.

Synthesis of {[Ag_2L(NO_3)$_2$]·H_2O}$_n$ (9): 0.5 mmol (100 mg) of (**1**) in 10 mL of HNO_3 0.1M were added in a round bottom flask wrapped with aluminum foil and refluxed under stirring during 2h. Then, 1 mmol (170 mg) of $AgNO_3$ was added and refluxed during 2 h. After that, the mixture was allowed to reach room temperature and the resulting precipitate was filtered-off. The clear solution was kept unperturbed and white needles of (**9**) appeared after 10 min (110 mg, 43%) and are filtered-off. The resulting transparent solution was again kept unperturbed during one month. New crystals

adequate for X-ray analysis appeared at the bottom of the flask (10 mg, 4%). The complex exhibits a weight loss between 50 and 180 ºC corresponding to one water molecule per formula unit [calc.: 3.2; found: 3.4%] and a final residue of Ag corresponding to 2 Ag per formula unit [calc.: 38.5; found: 38.2%]. IR (KBr, cm^{-1}): 3276m, 3201m, 1638s, 1587s, 1508s, 1449s, 1384m, 1328m, 1010w, 798w, 585w. ^{1}H NMR: This product is insoluble in the most common NMR solvents. ESI-HRMS: It has been impossible to obtain the corresponding ESI-HRMS. The product decomposes in solution and only the protonated ligand $[\mathbf{4} + H]^+$ is observed. No significant signals with Ag^+ have been detected.

X-ray crystallography

Crystallographic data for compounds (**1**–**3**), (**5**), (**7**) and (**9**) were acquired on Enraf Nonius CAD4 diffractometers, with Mo-Kα radiation (λ=0.71073 Å) using a graphite crystal monochromator at 21 ºC. X-ray diffraction data for compound (**4**) was collected on a Bruker-Nonius diffractometer equipped with an APPEX II 4K CCD area detector, a FR591 rotating anode with MoKα radiation, Montel mirrors, and a Kryoflex low-temperature device (T = -173 °C). Suitable crystals of (**6**) and (**8**) were selected for X-ray single crystal diffraction experiments, covered with oil (Infineum V8512, formerly known as Paratone N) and mounted at the tip of a nylon CryoLoop on a BRUKER-NONIUS X8 APEX KAPPA CCD diffractometer using graphite monochromated MoK_α radiation (λ = 0.71073 Å). Crystallographic data were collected at room temperature (27 ºC). Data were corrected for Lorentz and polarisation effects and for absorption by semiempirical methods based on symmetry-equivalent reflections [23] (**6** and **8**). All crystal structures were solved by direct methods, using the program SIR2014 [24] (**1**-**3**, **5**, **7** and **9**), SHELXT-2014 (**6** and **8**) and SIR2011 [25] (**4**). Refinement was made by full-matrix least squares on F2 with SHELXL-2017/1 [26-28] (**1**-**3** and **5**-**9**), running under the WinGX matrix [29], and SHELXL-2018/3 (**4**). The structures were checked for higher symmetry with help of the program PLATON. [30] All hydrogen atoms were considered as ideal and geometrically placed, except those of water molecules that were refined with restraints in such a manner that give rise to reasonable H-bonds in the crystal packing. Protonation sites were located in the Fourier difference maps prior to introduce the corresponding calculated hydrogens. A riding model with the anisotropic thermal vibration fixed at 1.2 times Uiso of the bonded atom was used for the H-atoms,

except for those bonded to heteroatoms (N, O), from which a thermal vibration of 1.5 times Uiso was used (**6** and **8**). Compounds (**1**) and (**5**) crystallize as monohydrates and the cocrystal (**3**) is a methanol solvate showing a half occupancy. In compound (**6**), the nitrate anion was split into five different positions (partial occupancy 30 %, 20 %, 20 %, 15 % and 15 %) to account for the rotation around of the molecule.

Publication materials were generated with WinGX [29]. Selected crystal and data collection parameters are reported in Electronic Support Information (Tables S1 and S2). X-ray crystallographic data for compounds 1-9 (CIF files) have been deposited with the Cambridge Crystallographic Data Centre, CCDC numbers 1943810-1943818. Copies of this information may be obtained free of charge from the Director, CCDC, 12 Union Road, Cambridge, CB2 1EZ, UK, (e-mail: deposit@ccdc.cam.ac.uk or www: http://www.ccdc.cam.ac.uk).

Theoretical methods

All DFT calculations were carried out using the Gaussian-09 program [31] at the B3LYP-D/def2-TZVP level of theory and using the crystallographic coordinates (only the position of the H-atoms has been optimized). Atoms-in-Molecules (AIM) [32] analysis was performed at the same level of theory. The calculation of AIM properties was done using the AIMAll program [33].

Molecular Docking calculations

The docking study was performed with the CDOCKER tool of Discovery Studio 2016 software (DS2016) [34]. The CDOCKER is a CHARMm-based docking algorithm that uses the CHARMm family of force fields and offers all the advantages of full ligand flexibility (including bonds, angles, and dihedrals) [35]. The CDOCKER algorithm adopts a strategy involving the generation of several initial ligand orientations in the binding site of DNA target followed by molecular dynamics-based simulated annealing and final refinement by energy [36]. Two Calf-Timus DNA models (ctDNA) were retrieved from the Protein Data Bank (PDB codes: 1BNA and 1CGC) [37,38] (Figure S1). The sequences of the ctDNA were $d(CGCGAATTCGCG)_2$ and $d(CCGGCGCCGG)_2$ respectively. The DNA models were prepared following the protocol: i) water molecules were deleted and hydrogen atoms were added and ii) DNA model were refined with CHARMm at physiological pH. Later, analysis of possible

DNA binding site was realized for docking and scoring applications. It defines a region in a model where binding interactions can occur. Four different regions were found in each case (Figure S1). Consequently, the inhibitors were docked into each of the binding sites. Ten conformations of each compound were obtained through CDOCKER. The $-E_{\text{CDOCKER}}$ is the interaction energy between the ligand and the receptor and the internal ligand strain energy. The $-E_{\text{CDOCKER\_IN}}$ includes only the interaction energy between the ligand and receptor. This enables the energies to be used as a score, where a higher value indicates more favorable binding. The conformations with lowest energy were selected as the most probable binding conformation for each compound.

Results and discussion

Synthesis of the compounds

We have synthesized compounds (**1**–**9**) by means of the general procedure shown in Scheme 1. It should be mentioned that the N^9-substituted compound (**2**) is obtained as a sub-product during the synthesis of (**1**), which is the major product. This result is independent of the reaction conditions (base and atmosphere conditions). Thus, the utilization of anhydrous K_2CO_3 or $CsCO_3$ instead of HNa and either in argon atmosphere or in the air yield the N^7-derivative as the main product. It is easy to distinguish between these two isomers by means ^{1}H-NMR because aromatic signals are very different. Thus, C8-H appears at 9.24s and 8.99s, and C2-H at 8.28s and 8.39s, for (**1**) and (**2**) respectively. This result is unexpected since adenine alkylation reactions usually lead to the N^9-substituted regioisomer as major product. Moreover, we would like to emphasize that co-crystal (**3**) was obtained serendipitously in one of our attempts to synthesize compound (**1**) where the starting product, adenine, was not totally consumed.

N^7-(2-pyrimidyl)-adenine (**1**) is not stable in acidic media (either HCl or HNO_3) under heating conditions (65–90ºC), yielding the corresponding *bis*-pyrimidyl-amine that can be obtained either as neutral compound (**4**) or monoprotonated (**6**) (nitrate salt) or diprotonated (**5** and **7**) (hydrochloride or tetrachloridozincate) forms (see Scheme 1). Thus, if NaOH is added to a solution of (**5**) (until pH = 12) then the neutral compound (**4**) is obtained. The ^{1}H-NMR shows the absence of peaks related to C8-H presented in (**1**) and only an aromatic signal is observed at 7.74s in neutral (**4**) or 8.19s to 8.24s in the corresponding protonated forms (**5**-**7**). Moreover, ^{13}C-NMR are in agreement with

the protonation, with more shielded peaks corresponding to Cα to protonated N (C2, C4, C5, C6, C2a, C4a, C6a). Therefore, this can be envisaged as a convenient and easy method to obtain N^5-(pyrimidin-2-yl)-pyrimidine-4,5,6-triamine. In fact, we have further used this molecule as ligand and synthesized the mononuclear Ir(III) complex (**8**) and the coordination Ag(I) polymer (**9**). Compound (**2**) was degraded under the same reaction conditions, giving rise to multiple byproducts in a non-selective manner. On the contrary, N^7-methyladenine turned out to be stable under the same reaction conditions, recovering the protonated adenine scaffold at the end of the reaction.

Description of the crystal structures

Crystal structures of compounds (1–3)

The N-pyrimidyl-adenines (**1**) and (**2**) crystallize in the monoclinic system with the P21/c space group and the co-crystal (**1**):adenine 1:1 (**3**) crystallizes in the monoclinic system with the C2/c space group. The X-ray structures are given in Figure 1 with the atom numbering scheme. Compound (**1**) presents an intramolecular N6–H···N1A H-bond that likely explains the fact that (**1**) is the major compound in the reaction of adenine with 2-chloropyrimidine. This aspect is further analyzed below. In compound (**3**), the 1:1 co-crystal is stabilized by the formation of two strong N6–H···N7B(adenine) and N6B(adenine)–H···N1 bonds in addition to the intramolecular N6–H···N1A one.

Insert here Figure 1

Infinite 1D supramolecular assemblies can be observed (see Figure 2a) in the solid state of (**1**). This assembly propagates by means of two types of H-bonding networks that are formed at opposite sides of (**1**), one highlighted in orange and the other one in green. The first one is formed through double N6–H···N1 hydrogen bonds (H···N distance 2.29 Å, Watson-Crick site of adenine moiety). At the other side, the N^7-substituted pyrimidine ring is involved in an H-bonding network where four C–H···N H-bonds are established (C8–H···N3A and C4A–H···N9, H···N distances of 2.60 and 2.73 Å respectively). In compound (**2**), such a polymeric 1D chain is not formed and simply self-assembled N6–H···N1 H-bonded dimers via the Watson-Crick site of adenine are formed (one dimer is shown in Figure 2b, H···N distance 2.19 Å). It is interesting to comment the H-bonding network in the co-crystal (**3**). An infinite 1D supramolecular tape is formed, where double N9B–H···N3B H-bonded self-assembled dimers of

adenine (highlighted in pink in Figure 2c) are inserted between self-assembled dimers of N^7-(2-pyrimidyl)-adenine (highlighted in green). The interaction of the self-assembled dimer of adenine with the adjacent N^7-(2-pyrimidyl)-adenine molecules is via the Hoogsteen faces of the dimer (highlighted in blue). In addition to the H-bonding interactions described in Figure 2, π-stacking forces are also crucial governing the final 3D solid-state structures of compounds (**1**–**3)** as described in the ESI (see Figures S2 to S4).

Insert here Figure 2

Crystal structure of compounds (4–6)

Single-crystal X-ray diffraction analyses reveal that compound (**4**) and (**5**) crystallize in the monoclinic system with the P21/n and P21/c space groups, respectively. Compound (**6**) crystallizes in the triclinic system with the P-1 space group. In compound (**4**), the asymmetric unit contains the ligand and one co-crystallized MeOH molecule (see Figure 3a). In compound (**5**) the asymmetric unit contains four chloride anions and two diprotonated H_2L^{2+} counter-cations (see Figure 3b) where each pyrimidinic ring of the ligand is protonated (in N1 and N1A). In compound (**6**), the asymmetric unit contains one nitrate anion and one monoprotonated ligand in N1 (see Figure 3c).

Insert here Figure 3

In the solid state of neutral (**4**) and monoprotonated (**6**) compounds, 1D supramolecular tapes are formed, as shown in Figure 4. In compound (**4**), the 1D assembly is governed by the formation of two H-bonds (N1–H···N3 and N4–H···N7 (see Figure 4a). The N5–H group does not participate because it is blocked by the MeOH molecule via the formation of a N5–H···O1 H-bond. In compound (**6**) the nitrate anion connects two HL^+ cations by means of the three oxygen atoms generating the infinite 1D tapes. It forms two strong hydrogen bonds with the protonated N1–H and the exocyclic N6–H groups of one ligand using the O21 and O23 atoms and with the N7–H group of the adjacent ligand via the O22 atom (see Figure 4b). In both compounds the tapes are interconnected by means of an intricate combination of interactions (H-bonds and π-stacking) as further described in the ESI (see Figure S5).

Insert here Figure 4

On the other hand, in the solid-state structure of (**5**), the chloride anions are stabilized by a combination of H-bonding and anion–π interactions. It has been previously

demonstrated that protonated diazines and triazines are excellent aromatic anion–π acceptors due to the enhanced π-acidity of the ring due to the protonation [39,40]. In addition, the combination of H-bonds and anion–π interactions has been used as a strategy for the synthesis of receptors adequate for anion recognition [41]. Figure 5 shows both types of anion–π interactions observed in compound (**5**). The geometric features of both complexes are very similar with respect to the H-bond/anion–π interaction with Cl1/Cl2. The main difference is that in one case (Figure 5a) the N6–H and N1–H groups interact with a chloride anion and in the other one the N9–H and N3B–H groups interact with the co-crystallized water molecule (Figure 5a).

Insert here Figure 5

Crystal structure of $(H_2L)(ZnCl_4)$ (7)

The X-ray structure of compound (**7**), which crystallizes in the monoclinic P21/c crystal system, is shown in Figure 6. The asymmetric unit consists of one $[ZnCl_4]^{2-}$ anion and the diprotonated H_2L^{2+} cation in N1 and N3A.

** Insert here Figure 6**

The solid-state structure of (**7**) possesses several supramolecular assemblies through a combination of hydrogen bonding or/and anion–π interactions. Figure 7a shows a self-assembled tetramer formed by two $[ZnCl_4]^{2-}$ anions and two H_2L^{2+} molecules. In the tetramer a network of N–H···Cl H-bonding interactions is formed where Cl3 and Cl4 atoms are accommodated through bifurcated N–H···Cl hydrogen bonds (H···Cl distances 2.30 and 2.61 Å). Moreover, in Figure 7b we show another assembly where the $[ZnCl_4]^{2-}$ anion establishes two H-bonds with one exocyclic NH_2 group (highlighted in green) and also forms an anion–π interaction with Cl4 atom. A differential feature with respect to the hydrochloride compound (**5**), is that the anion–π interaction is established with the pyrimidine instead of the diaminopyrimidine ring (see Figure 5).

** Insert here Figure 7**

Crystal structures of $[Ir(L)(DMSO\text{-}\kappa S)(Cl)_3]$ (8) and $\{[Ag_2L(NO_3)_2]\cdot H_2O\}_n$ (9)

Compounds (**8**) and (**9**) crystallize in the monoclinic space groups P21/c and P21/n, respectively. Their X-ray structures are shown in Figure 8 and the coordination sphere (distance/angle) of both complexes is given in Table 1. It can be observed that the Ir(III)

complex (**8**) is mononuclear and monomeric and the Ag(I) complex (**9**) is a coordination polymer.

Insert here Table 1

In compound (**8**), the Ir(III) is hexacoordinated to the N1A and N7 atoms of the ligand, three chlorine atoms and one DMSO. It should be mentioned that although the synthesis of this complex is made in an acidic medium, the resulting zwitterionic complex shows deprotonation in the amine group N7, and protonation in N1. The deprotonation in N7 is quite unexpected taking into consideration the acidic reaction conditions. In the solid state it forms infinite 1D supramolecular chains where two types of π-stacking interactions are established (see Figure 9a). In one of them (in green) the protonated diaminopyrimidine rings are anti-parallel stacked and also establish H-bonding interactions with the O-atom of the coordinated DMSO. In the stacking interaction only two C-atoms overlap with a C···C distance of 3.35 Å. In the other π–π interaction (in orange), the Ir(III)–coordinated pyrimidine rings are also stacked in an anti-parallel mode with a larger overlap of the π-systems. The antiparallel nature of the stacking complexes observed in (**8**) is favored to maximize the dipole···dipole interaction.

In compound (**9**), the neutral ligand is coordinated to four Ag(I) atoms via the four pyrimidinic N-atoms (N3, N3A, N1 and N1A). The nitrate counter ions are directly coordinated to the Ag either monodentate or bidentate (see Figure 8b). As usual, the Ag–N coordination distances (see Table 3) are significantly shorter than the Ag–O ones.

** Insert here Figure 8**

Compound (**9**) is a 2D coordination polymer (see Figure 9b) where neither large cavities nor channels are formed. The final 3D solid state architecture is formed by the assembly of the 2D layers by means of H-bonds involving the co-crystallized water molecules as described in the ESI (see Figure S6). In Figure 9c we highlight several H-bonds that are formed between the amino group and the nitrate anions that further contribute to the stabilization of the 2D layer.

** Insert here Figure 9**

Theoretical DFT study

In this part of the manuscript we analyze the interesting H-bonding network observed in the solid state of N^7-(2-pyrimidyl)-adenine (**1**) and the co-crystal (**1**):adenine (**3**). The

H-bonding pattern observed in (**2**) is equivalent to (**1**). In particular, we are interested in the evaluation and comparison of the interaction energy of each H-bond. Therefore, we have used the QTAIM method and the value of the kinetic $G(r_{CP})$ contribution to the local energy density of electrons at the critical point (CP). This method is helpful to compute the stabilization energy that accounts for each individual H-bonding contact since it was specifically developed for HBs by Vener and coworkers [42] [Energy = 0.429 * G(r) at the bond CP]. We have recently applied this methodology [21] in H-bonded assemblies of hybrid adenine-β-alanine and adenine-GABA molecules and shown that the results are very similar to those computed using standard complexation energies.

Figure 10 shows the distribution of critical points and bond paths of the self-assembled N6–H···N1 dimer of compound (**1**) and a trimer of compound (**3**), that allow us to compare the different binding modes commented above for compounds **1**–**3**. First, it is interesting to comment that the energy of the intramolecular (N6-H···N1A) H-bond is 5.08 kcal/mol in (**1**) and 5.90 kcal/mol in (**3**). This extra stabilization energy is probably responsible for the preference of N7-substitution instead of N9 in the reaction of adenine with 2-chloropyrimidine. Moreover, the stabilization energy associated to each intermolecular N6–H···N1 H-bond in (**1**) is 2.90 kcal/mol. The AIM analysis of (**3**) shows that the C–H···N9 and C–H···N3A are energetically weaker, 1.32 and 1.94 kca/mol respectively. However, globally the formation energy of the dimer with four C–H···N bonds is 6.52 kcal/mol, therefore more stable than the N6–H···N1 dimer in (**1**) (5.80 kcal/mol). The energetic features of the H-bonds between the adenine (Hoogsteen face) and N^7-pyrimidyladenine (Watson-Crick face) are 3.70 kcal/mol for N6(adenine)–H···N1 and 4.15 kcal/mol for N6–H···N7(adenine). Therefore, the total stabilization for this particular complex is 7.85 kcal/mol, which is stronger than that for the self-assembled N6–H···N1 dimer of (**1**). This likely explains the fact that the N6–H···N1 dimer observed the X-ray structure of (**1**) is not preserved in the co-crystal (**3**), and, instead, the insertion of adenine dimers occurs. Actually, the most stable assembly corresponds to the adenine dimer that is formed via two symmetrically related N9–H···N3 H-bonds (5.56 kcal/mol each H-bond). This energetic analysis reveals that the self-assembled N9–H···N3 adenine dimer is a very robust synthon that is inserted in the infinite tape of (**1**) because the H-bonds are replaced by stronger ones via the Hoogstein(adenine)···Watson-Crick(N^7-pyrimidyladenine) interaction

** Insert here Figure 10**

Molecular Docking with DNA

We have studied theoretically the affinity of the N-(2-pyrimidyl)adenines (**1**) and (**2**), the bis-pyrimidyl-amine (**4**(**L**)), the monoprotonated bis-pyrimidyl-amine (**6**) and the Ir(III) complex (**8**) to DNA in order to investigate their possible use as antiproliferative drugs. Two Calf-Timus DNA models (ctDNA) were retrieved from the PDB as described in the theoretical methods. Four different regions were found in each ctDNA model suitable for docking as shown in Figure S1. Consequently, the compounds were docked into each of the binding sites (BS) by using ten possible conformations of each compound. The $-E_{\mathrm{CDOCKER\_IN}}$ term denotes the interaction energy between the compound and the DNA model and the $-E_{\mathrm{CDOCKER}}$ includes an additional term that accounts for the internal strain energy, which is the energy associated to the deformation of both the DNA and the ligand upon complexation. As a first approximation we use $-E_{\mathrm{CDOCKER\_IN}}$ term to discriminate between the four possible BSs detected by the program. Moreover, the conformations with lowest energy are selected as the most probable binding conformation for each compound. The results are summarized in Table 2 and they clearly indicate that bis-pyrimidyl-amines (compounds **4** and **6**) have a good affinity for the minor groove BSs of the DNA models. The protonated form presents the high $-E_{\mathrm{DOCKER}}$ values of 37.32 kcal/mol^{-1} for 1BNA model and 40.48 kcal/mol for 1CGC model. It is also interesting to comment that the $-E_{\mathrm{CDOCKER\_IN}}$ and $-E_{\mathrm{CDOCKER}}$ terms in compound **6** are very similar, thus indicating that the strain (deformation) energy is very small. In contrast, for compounds **1** and **2**, the deformation energy is large since the $-E_{\mathrm{CDOCKER}}$ term is significantly smaller compared to $-E_{\mathrm{CDOCKER\_IN}}$. A general trend is that all compounds exhibit larger affinity for the binding sites located at the minor groove of DNA and there is not a significant difference between the DNA rich in GC pairs and that rich in AT pairs. It is worth mentioning that the Ir complex **8** presents negative values (no effective binding) of $-E_{\mathrm{CDOCKER}}$ term in all binding sites and the two models of DNA thus indicating that the deformation energy required for the complexation is too large, which largely compensates the interaction energy ($-E_{\mathrm{CDOCKER\_IN}}$). Figure 11 (top) presents the preferred binding site for 1BNA model with the best inhibitor (compound **6**). It preferentially binds the AT rich domain of the minor groove. The type and bonding distances of the non-covalent interactions is given in Tables S3 and S4. All hydrogen-bond interactions are moderately strong, and

the inhibitor has a π-sigma type interaction between the pyrimidine ring and thymine base (see Table S3). In a similar way, Figure 11 (bottom) shows the docked compound **6** in the CG rich region of minor groove of 1CGC model. In this case all the interactions are hydrogen bonds that are established preferentially with the guanine bases 3, 4, 19 and 20, as detailed in Table S2.

** Insert here Figure 10**

** Insert here Table 2**

Conclusions

We have synthesized and X-ray characterized nine adenine-pyrimidine derivatives. Unexpectedly, the regioselectivity of adenine was reverse with respect to published results and the N^7-substituted product was the major isomer due to the formation of a intramolecular H-bond. Also unexpectedly, this regioisomer is not stable under acidic conditions and a new *bis*-pyrimidine ligand is formed. This ligand has been X-ray characterized in its neutral form, protonated and diprotonated. Furthermore, an outer sphere complex of $H_2\mathbf{L}^{2+}$ with $[ZnCl_4]^{2-}$ has been also characterized. Finally, inner sphere complexes with Ir(III) and Ag(I) have been obtained. The latter is a 2D coordination polymer. Molecular docking experiments using two models of DNA suggest that the protonated *bis*-pyrimidine ligand has a strong ability to interact with the minor groove of DNA, therefore it is a good candidate to further experiments. In contrast the Ir(III) complex does not have affinity for the DNA if the deformation energy is taken into account. Finally, we have computed the interaction energy of the individual H-bonding interactions observed in the solid state of N7-(2-pyrimidyl)adenine (**1**) and the co-crystal of (1):adenine (**3**) that lead to the formation of infinite 1D assemblies in their solid state structure. The energetic study might be useful to predict co-crystallization modes of adenine derivatives.

Acknowledgements

We thank the MINECO/AEI from Spain for financial support (project numbers CTQ2017-85821-R, ENE2015-63969-C3-3-R, BIO2016-78057-R and SEV2015-0496, FEDER funds and CTQ2017-90802-REDT). We also thank the Direcció General de Recerca i Innovació del Govern Balear (AAEE039/2017) for funding. We thank the CTI (UIB) for computational

facilities and allocation of computer time. We thank the Vice-Rector for Research and International Relations of the University of the Balearic Islands for the financial support in setting up the single-crystal X-ray diffraction facility.

References

[1] D. M Huryn, M. Okabe, Chem. Rev. 92 (1992) 1745-1768.

[2] A. Holy, in Advances in Antiviral Drug Design, vol. 1, E. De Clerq (ed.). JAI Press: Greenwich, CT, 1993; 179 – 232.

[3] A. Holy, H. Dvorakova, J. Jindrich, in: K. Krohn, H.A. Kirst, H. Maag (Eds). Antibiotics and Antiviral Compounds, VCH, Weinheim, 1993.

[4] F. Seela, H. Winter, Helv. Chim. Acta 77 (1994) 597-607.

[5] R.J. Rousseau, R.K. Robins, L.B. Townsend, J. Am. Chem. Soc. 90 (1968) 2661-2668.

[6] NJ Leonard, T. Fujii, T. Saito Chem. Pharm. Bull. 34 (1986) 2037-2043.

[7] D. Hockova, M. Masojıdkova, A. Holy, Collect. Czech. Chem. Commun. 64 (1999) 1316-1324.

[8] J. Boroski, Nucleosides & Nucleotides 15 (1996) 771-791.

[9] A. Garcia-Raso, J.J. Fiol, F.M. Alberti, Y. Lagos, M. Torres, M. Barceló-Oliver, M.J. Prieto, V. Moreno, I. Mata, E. Molins, C. Estarellas, A. Frontera, D. Quinonero, P.M. Deya, Eur. J. Inorg. Chem. 2010 (2010) 5617–5628.

[10] A. Garcia-Raso, F.M. Alberti, J.J. Fiol, Y. Lagos, M. Torres, E. Molins, I. Mata, C. Estarellas, A. Frontera, D. Quinonero, P.M. Deya, Eur. J. Org. Chem. 2010 (2010) 5171–5180.

[11] A. Garcia-Raso, F.M. Alberti, J.J. Fiol, A. Tasada, M. Barceló-Oliver, E. Molins, D. Escudero, A. Frontera, D. Quinonero, P.M. Deya, Inorg. Chem. 46 (2007) 10724–10735.

[12] S. Raic, M. Pongracic, J. Vorkapic-Furac, D. Vikic-Topic, A. Hergold-Brundic, Nucleosides Nucleotides 15 (1996) 937-960.

[13] A. Hasan, P.C. Srivastava, J. Med. Chem. 35 (1992) 1435-1439.

[14] L. Svansson, J. Kvarström J. Org. Chem. 56 (1991) 2993-2997.

[15] K. Okumura, T. Oine, Y. Yamada, M. Tomie, T. Adachi, T. Nagura, M. Kawazu, T. Mizoguchi, I. Inoue, J. Org. Chem. 36 (1971) 1573-1579.

[16] D. Hocková, M. Masojídková, M. Budesínský, A. Holý, Collect. Czech. Chem. Commun. 60 (1995) 224-236.

[17] A. Holý, H. Dvoráková, J. Jindrich, M. Masojídková, M. Budesínský, J. Balzarini, G. Andrei, E. De Clercq, J. Med. Chem. 39 (1996) 4073-4088.

[18] D. Hocková, M. Budesínský, R. Marek, J. Marek, A. Holý, Eur. J. Org. Chem. 1999 (1999) 2675-2682.

[19] A. García-Raso, C. Cabot, J.J. Fiol, L. Spichal, J. Nisler, A. Tasada, J.M. Luna, F.M. Albertí, I.V. Sibole, J. Plant Physiol. 14 (2009) 1529–1536.

[20] A. García-Raso, A. Terrón, A. Bauzá, A. Frontera, J.J. Molina, E.M. Vázquez-López, J. J. Fiol, New J. Chem. 42 (2018) 14742–14750.

[21] A. García-Raso, A. Terrón, A. Lopez-Zafra, A. Garcia-Viada, A. Barta, A. Frontera, J. Lorenzo, S. Rodriguez-Calado, E.M. Vázquez-López, J.J. Fiol, New J. Chem. 43 (2019) 9680–9688.

[22] R.Y. Schmitz, F. Skoog, A.V. Graham, C. Walker, L.H. Kirkegaard. N.J. Leonard, Phytochem. 14 (1975) 1479–1484.

[23] SADABS, Bruker-AXS, Version 1, Bruker AXS Inc., Madison, WI, 2004.

[24] M.C. Burla, R. Caliandro, B. Carrozzini, G.L. Cascarano, C. Cuocci, C. Giacovazzo, M. Mallamo, A. Mazzone, G. Polidori, J. Appl. Crystallogr., 48 (2015) 306-309.

[25] M.C. Burla, R. Caliandro, M. Camalli, B. Carrozzini, G.L. Cascarano, C. Giacovazzo, M. Mallamo, A. Mazzone, G. Polidori, R. Spagna, J. Appl. Cryst. 45 (2012) 351-356.

[26] G.M. Sheldrick, Acta Crystallogr., A64 (2008) 112-122.

[27] G.M. Sheldrick, Acta Crystallogr., C71 (2015) 3–8.

[28] G.M. Sheldrick, SHELXL-2017/1, Program for the Solution of Crystal Structures, University of Göttingen, Germany, 2017.

[29] L.J. Farrugia, J. Appl. Crystallogr. 32 (1999) 837-838.

[30] A.L. Spek, J. Appl. Crystallogr. 36 (2003) 7–13.

[31] Gaussian 09, Revision C.01, M.J. Frisch, G. W. Trucks, H.B. Schlegel, G. E. Scuseria, M.A. Robb, J.R. Cheeseman, G. Scalmani, V. Barone, B. Mennucci, G. A. Petersson, H. Nakatsuji, M. Caricato, X. Li, H.P. Hratchian, A.F. Izmaylov, J. Bloino, G. Zheng, J.L. Sonnenberg, M. Hada, M. Ehara, K. Toyota, R. Fukuda, J. Hasegawa, M. Ishida, T. Nakajima, Y. Honda, O. Kitao, H. Nakai, T. Vreven, J.A. Montgomery, Jr., J. E. Peralta, F. Ogliaro, M. Bearpark, J.J. Heyd, E. Brothers, K.N. Kudin, V.N. Staroverov, R. Kobayashi, J. Normand, K. Raghavachari, A. Rendell, J.C. Burant, S.S. Iyengar, J. Tomasi, M. Cossi, N. Rega, J.M. Millam, M. Klene, J.E. Knox, J.B. Cross,

V. Bakken, C. Adamo, J. Jaramillo, R. Gomperts, R. E. Stratmann, O. Yazyev, A.J. Austin, R. Cammi, C. Pomelli, J.W. Ochterski, R.L. Martin, K. Morokuma, V.G. Zakrzewski, G.A. Voth, P. Salvador, J.J. Dannenberg, S. Dapprich, A.D. Daniels, Ö. Farkas, J.B. Foresman, J.V. Ortiz, J. Cioslowski, D. J. Fox, Gaussian, Inc., Wallingford CT, 2009.

[32] R.F.W. Bader, J. Phys. Chem. A 102 (1998) 7314–7323

[33] T.A. Keith, AIMAll (Version 13.05.06), TK Gristmill Software, Overland Park, KS, 2013.

[34] G. Wu, D.H. Robertson, C.L. Brooks III; M. Vieth, J. Comp. Chem. 24 (2003) 1549-1562.

[35] B.R. Brooks, R.E. Bruccoleri, B.D. Olafson, D.J. States, S.A. Swaminathan, M. Karplus, J. Comput. Chem. 4 (1983) 187–217.

[36] S.L. Mo, W.F. Liu, C.G. Li, Z.W. Zhou, H.B. Luo, H. Chew, J. Liang, S. F. Zhou, Curr. Pharmaceut. Biotechnol. 13 (2012) 1640–1704.

[37] H.R. Drew, R.M. Wing, T. Takano, C. Broka, S. Tanaka, K. Itakura, R.E. Dickerson, Proc. Natl. Acad. Sci. USA. 78 (1981) 2179–2183.

[38] U. Heinemann, C. Alings, M. Bansal, EMBO J. 11 (1992) 1931–1939.

[39] P. Manna, S.K. Seth, M. Mitra, S.R. Choudhury, A. Bauza, A. Frontera, S. Mukhopadhyay, Cryst. Growth Des. 14 (2014) 5812–5821.

[40] P. Manna, S.K. Seth, A. Bauza, M. Mitra, S.R. Choudhury, A. Frontera, S. Mukhopadhyay, Cryst. Growth Des. 14 (2014) 747–755.

[41] L. Adriaenssens, G. Gil-Ramirez, A. Frontera, D. Quinonero, E.C. Escudero-Adan, P. Ballester, J. Am. Chem. Soc. 136 (2014) 3208–3218.

[42] M.V. Vener, A.N. Egorova, A.V. Churakov, V.G. Tsirelson, J. Comput. Chem. 33 (2012) 2303–2309

Table 1. Ir(III) and Ag(I) coordination distances (Å) and angles (º) in compounds (**8**) and (**9**) respectively. See Figure 8 for atom labeling scheme.

Ir(III) Compound (**8**)					
Atom Labels	Distance	Atom Labels	Angle	Atom Labels	Angle
Ir1–S1	2.227(1)	S1–Ir1–Cl3	95.50(4)	Cl2–Ir1–Cl3	90.19(4)
Ir1–Cl2	2.355(1)	S1–Ir1–Cl2	93.65(4)	Cl2–Ir1–N1A	101.8(1)
Ir1–Cl3	2.362(1)	S1–Ir1–N7	101.4(1)	Cl2–Ir1–N7	165.0(1)
Ir1–Cl1	2.342(1)	S1–Ir1–N1A	164.5(1)	Cl3–Ir1–Cl1	174.07(4)
Ir1–N1A	2.083(4)	S1–Ir1–Cl1	90.37(4)	Cl3–Ir1–N1A	86.2(1)
Ir1–N7	2.063(4)	N1A–Ir1–N7	63.2(1)	Cl3 Ir1–N7	88.7(1)
		Cl2–Ir1–Cl1	90.30(4)	Cl1–Ir1–N1A	88.0(1)
				Cl1–Ir1–N7	89.3(1)
Ag(I) polymeric compound (**9**)					
Atom Labels	Distance	Atom Labels	Angle	Atom Labels	Angle
Ag1–N1	2.205(5)	O1–Ag1–N3A	87.3(2)	N1A–Ag2–O5	87.4(2)
Ag1–O1	2.453(6)	O1–Ag1–N1	127.9(2)	N1A–Ag2–O6	107.2(2)
Ag1–N3A	2.239(5)	N3A–Ag1–N1	144.7(2)	O5–Ag2–O6	47.4(2)
Ag2–N1A	2.231(5)	N1A–Ag2–N3	148.2(2)	O5–Ag2–N3	122.9(2)
Ag2–O5	2.645(6)			O6–Ag2–N3	101.5(2)
Ag2–O6	2.697(5)				
Ag2–N3	2.201(4)				

Table 2. Docking analysis of several compounds in 1BNA and 1CGC PDB models (*binding sites in the minor groove) (score units: kcal/mol)

Compound	BS1		BS2*		BS3		BS4*	
	E_{DOCK}	E_{DOCK_IN}	E_{DOCK}	E_{DOCK_IN}	E_{DOCK}	E_{DOCK_IN}	E_{DOCK}	E_{DOCK_IN}
				1BNA				
1	6.04	16.87	13.93	24.75	6.38	17.30	9.86	21.15
2	8.14	18.93	14.55	25.44	-	-	9.87	20.74
4 (L)	25.15	17.30	28.70	21.40	23.97	16.45	29.24	22.57
6	30.21	27.56	**37.32**	37.71	27.45	24.42	32.44	29.83
8	<0	37.9	<0	48.5	-	-	<0	39.6
				1CGC				
1	7.42	18.49	8.79	19.63	7.12	18.31	6.89	18.25
2	8.32	19.07	11.51	22.35	8.26	19.04	7.49	18.40
4 (L)	29.29	22.11	33.74	25.91	25.82	17.92	27.81	20.27
6	36.34	33.81	**40.48**	38.21	27.16	25.67	31.05	28.25
8	<0	49.2	<0	47.2	<0	34.2	<0	40.0

Figures:

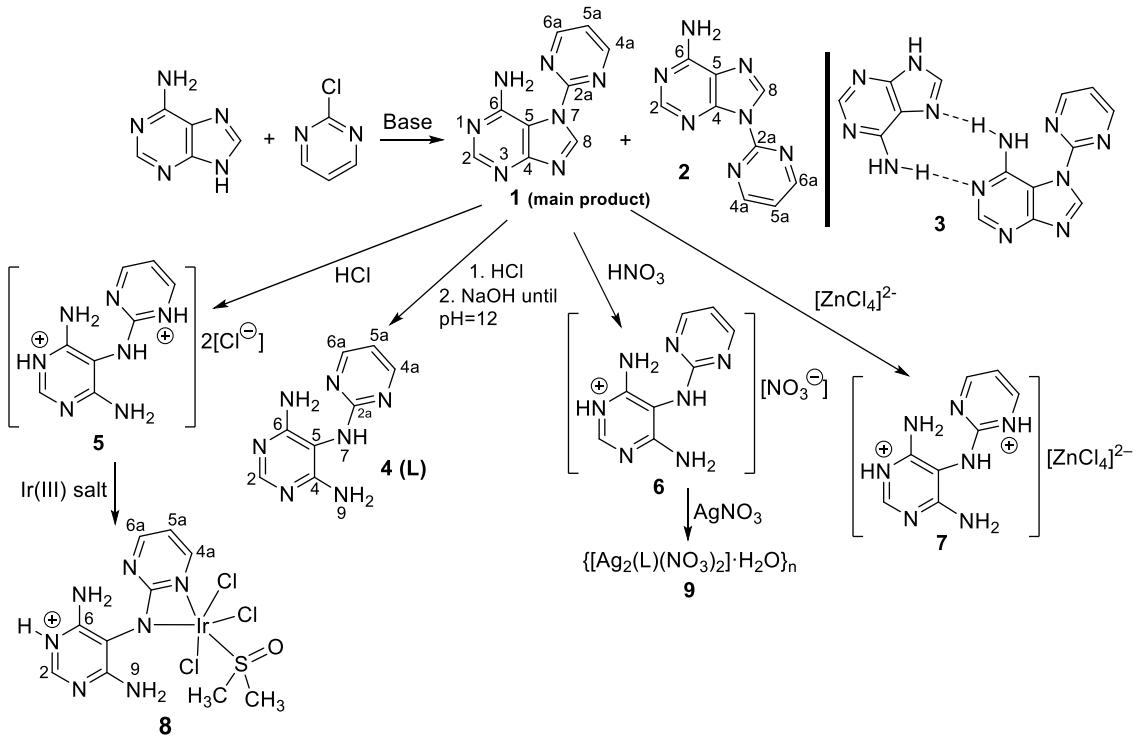

Scheme 1. Synthetic route to compounds (**1**–**9**).

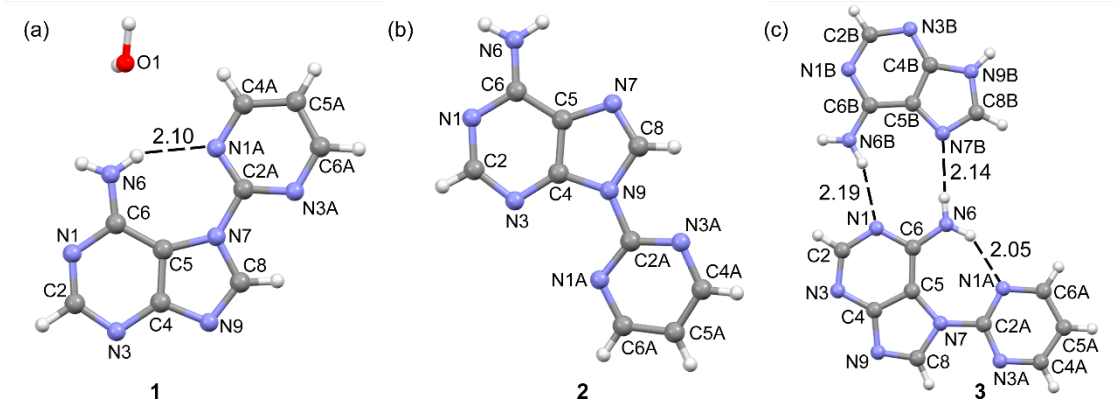

Figure 1. Asymmetric units of the X-ray structures of compounds (**1**) (a), (**2**) (b) and co-crystal (**3**) (c) including the atom numbering scheme. In (**3**), a disordered MeOH molecule has been omitted for clarity.

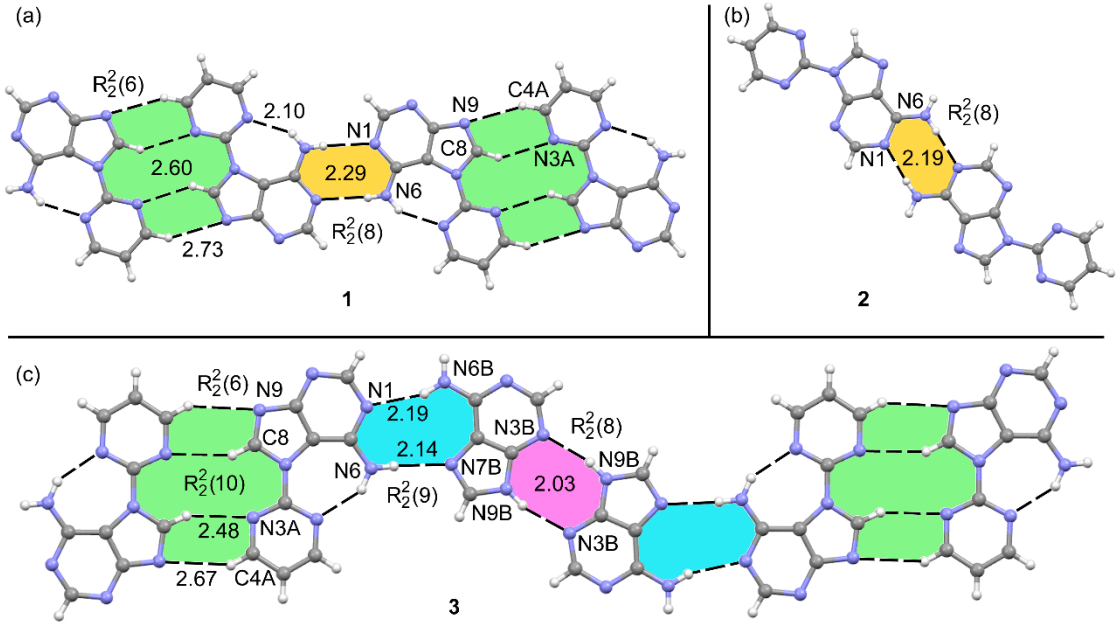

Figure 2. Several H-bonding networks observed in the X-ray structures of (**1**) (a), (**2**) (b) and co-crystal (**3**) (c). Distances in Å.

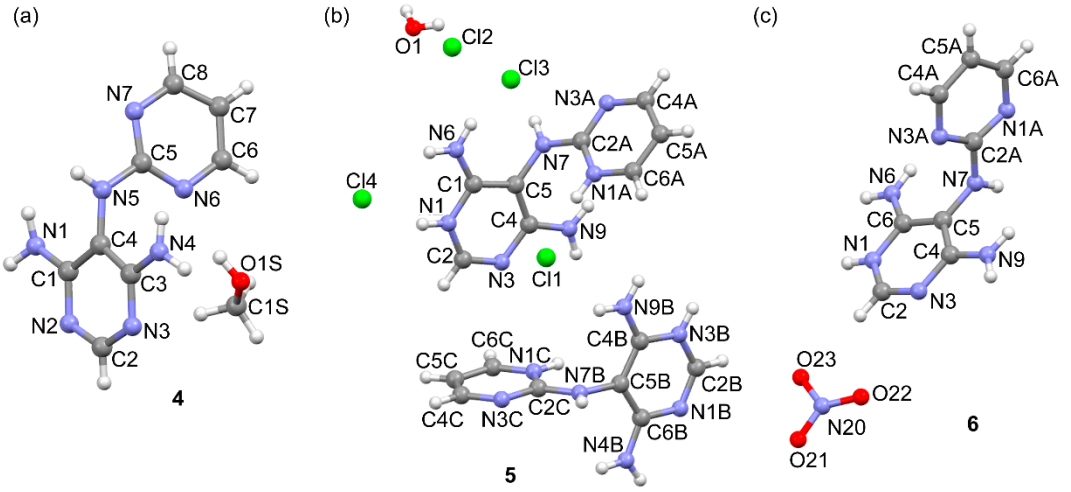

Figure 3. X-ray structures of compounds (**4**) (a), (**5**) (b) and (**6**) (c) including the atom numbering scheme. In (**6**), the anion is disordered and only a position (occupancy 30%) is given for clarity.

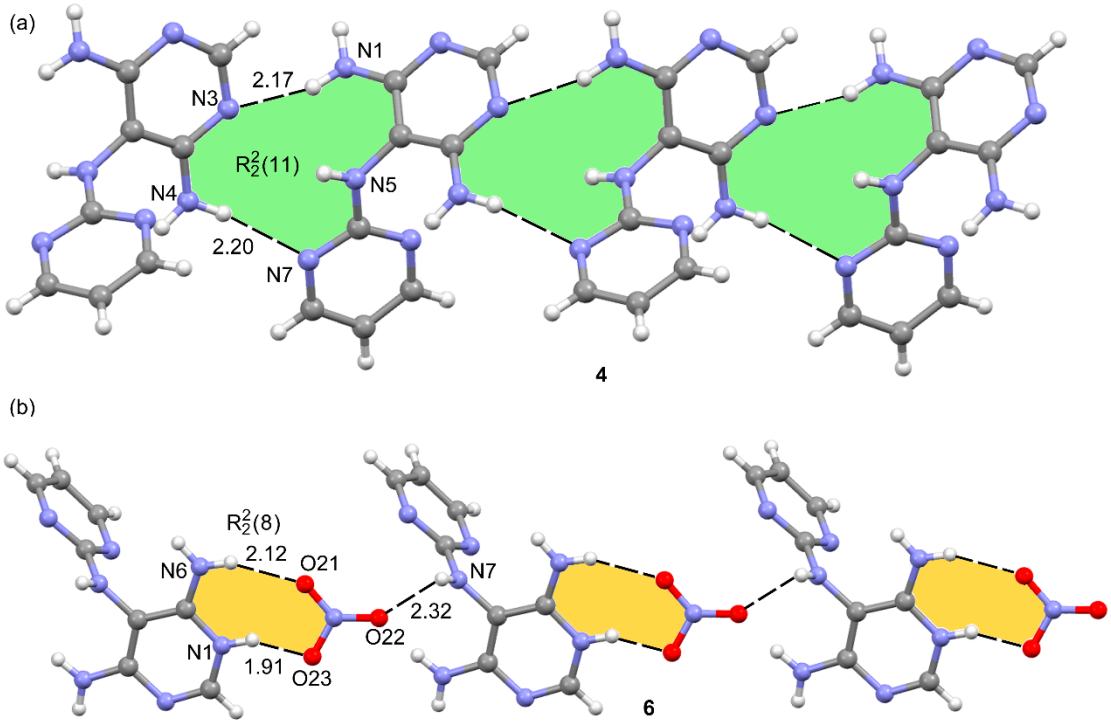

Figure 4. Infinite 1D tapes observed in the solid state of (**4**) (a) and (**6**) (b). Distances in Å.

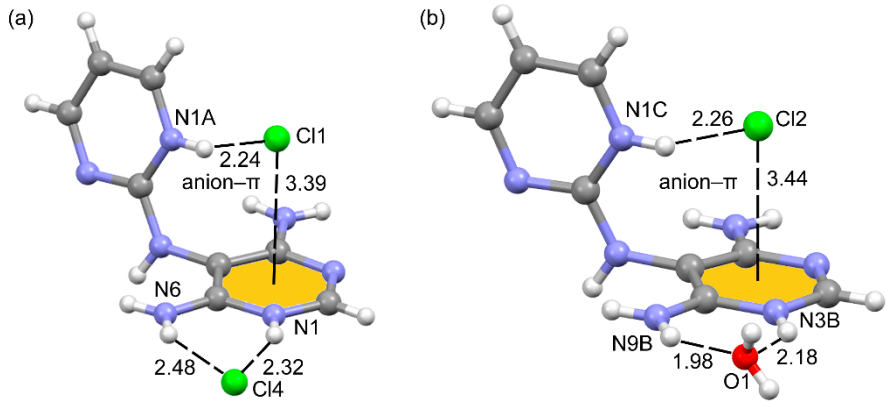

Figure 5. Two types of anion–π/H-bond complexes observed in the solid state of compound (**5**).

Distances in Å.

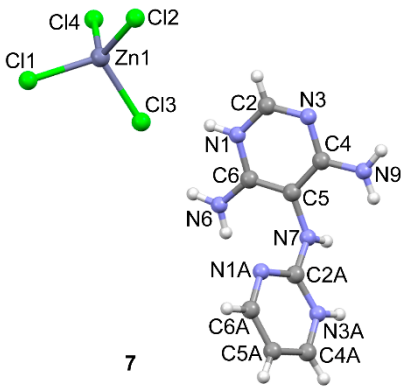

Figure 6. X-ray structure of compound (**7**) and the numbering scheme.

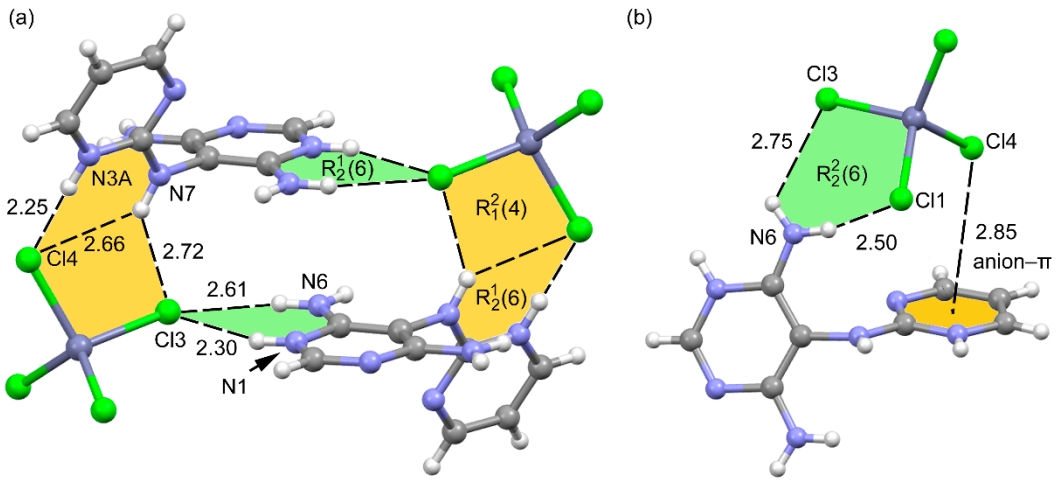

Figure 7. Two X-ray fragments of compound (**7**): self-assembled tetramer (a) and anion–π assembly (b). Distances in Å.

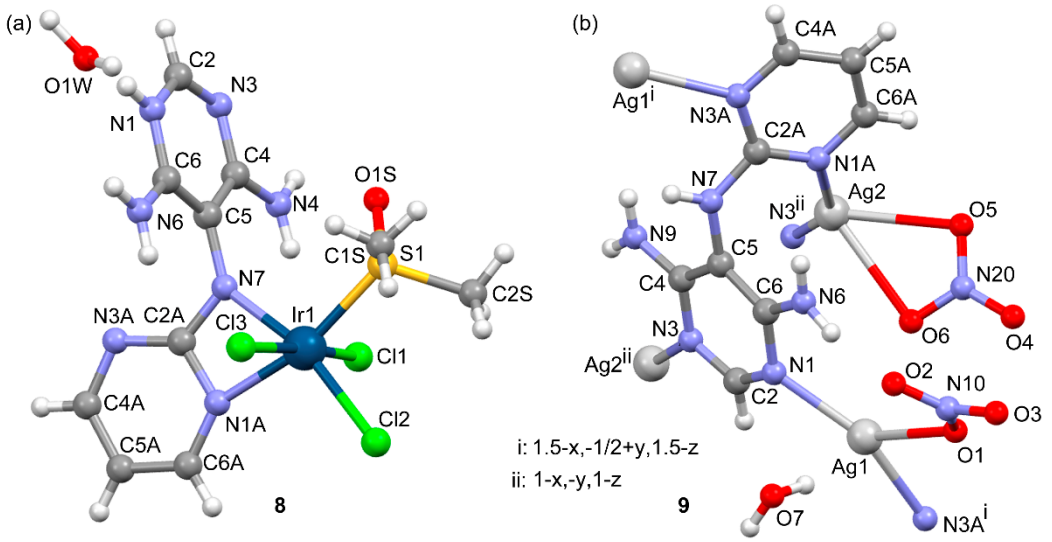

Figure 8. X-ray structures of compounds (**8**) (a) and (**9**) (b) including the atom numbering scheme.

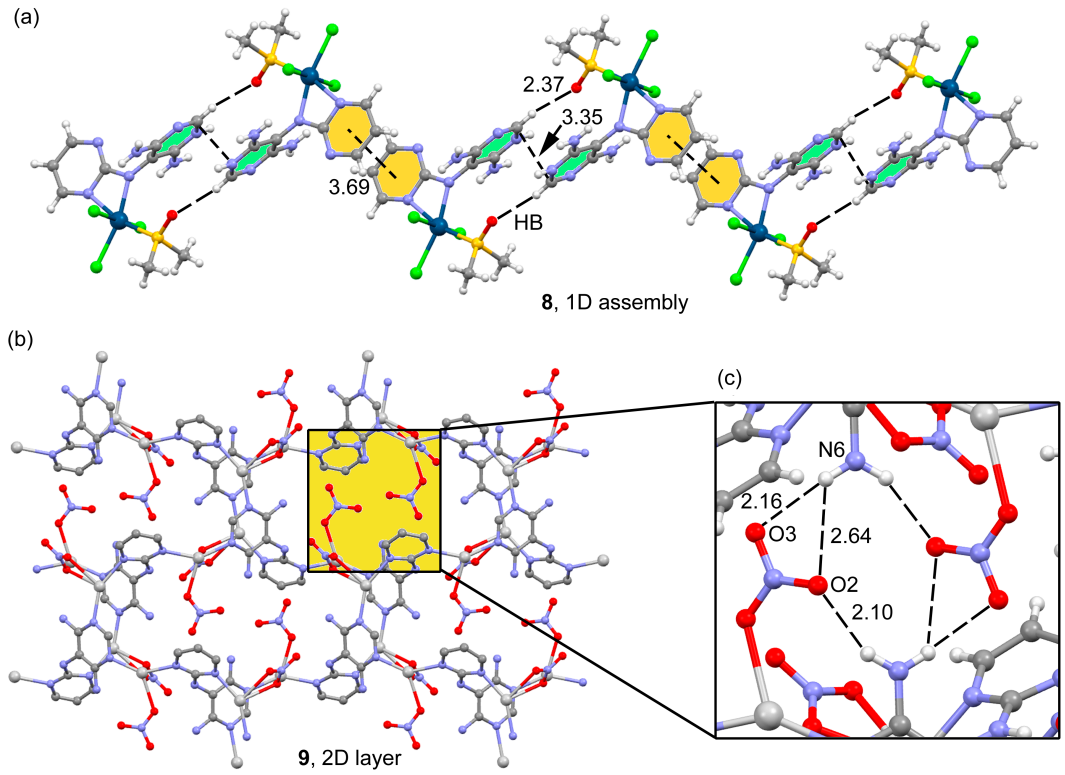

Figure 9. (a) Representation of the 1D assembly of compound (**8**) with indication of the two types of π-stacking interactions. (b) Representation of the 2D coordination polymer (**9**). H-atoms omitted for clarity. (c) Detail of the H-bonding network with the participation of the amino group and the nitrate counterions. Distances in Å.

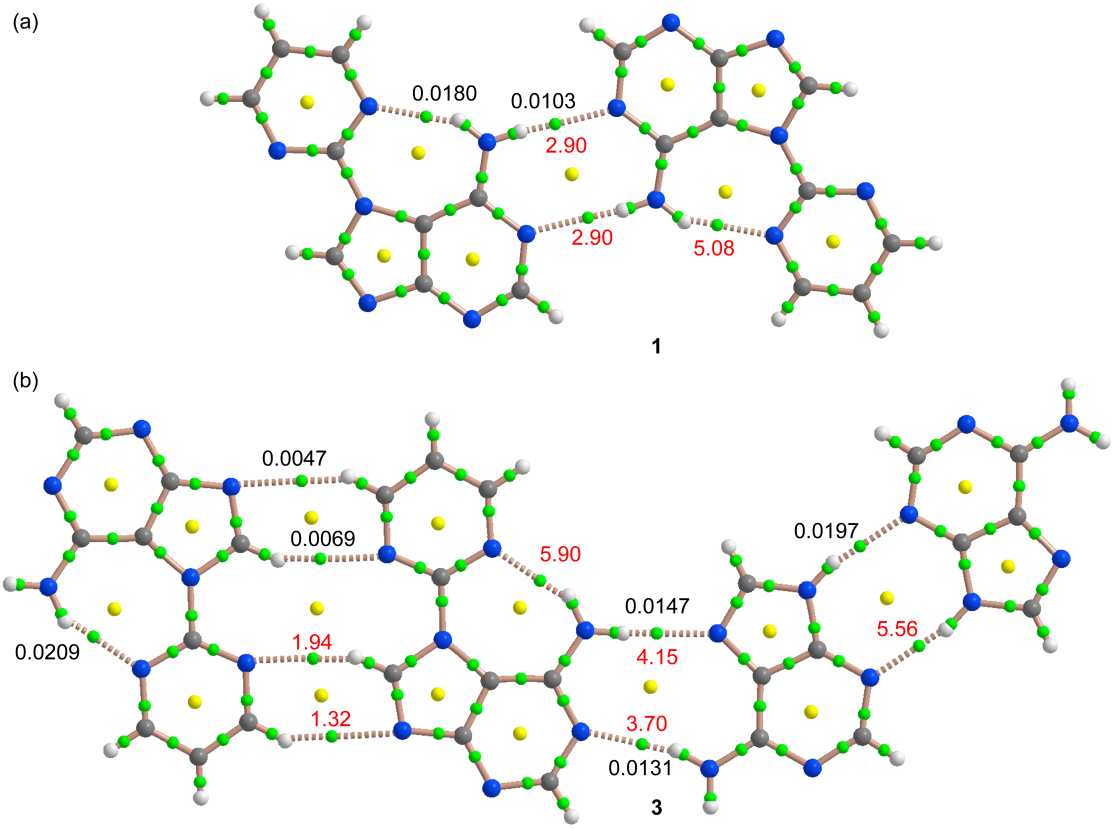

Figure 10. AIM distribution of bond and ring critical points (green and yellow spheres, respectively) and bond paths obtained for a dimers of compound (**1**) (a) and a trimer of compound (**3**) The dissociation energy of the H-bond using the G(r) values at the bond CP are indicated in red (kcal/mol) and the values of G(r) in black (a.u.).

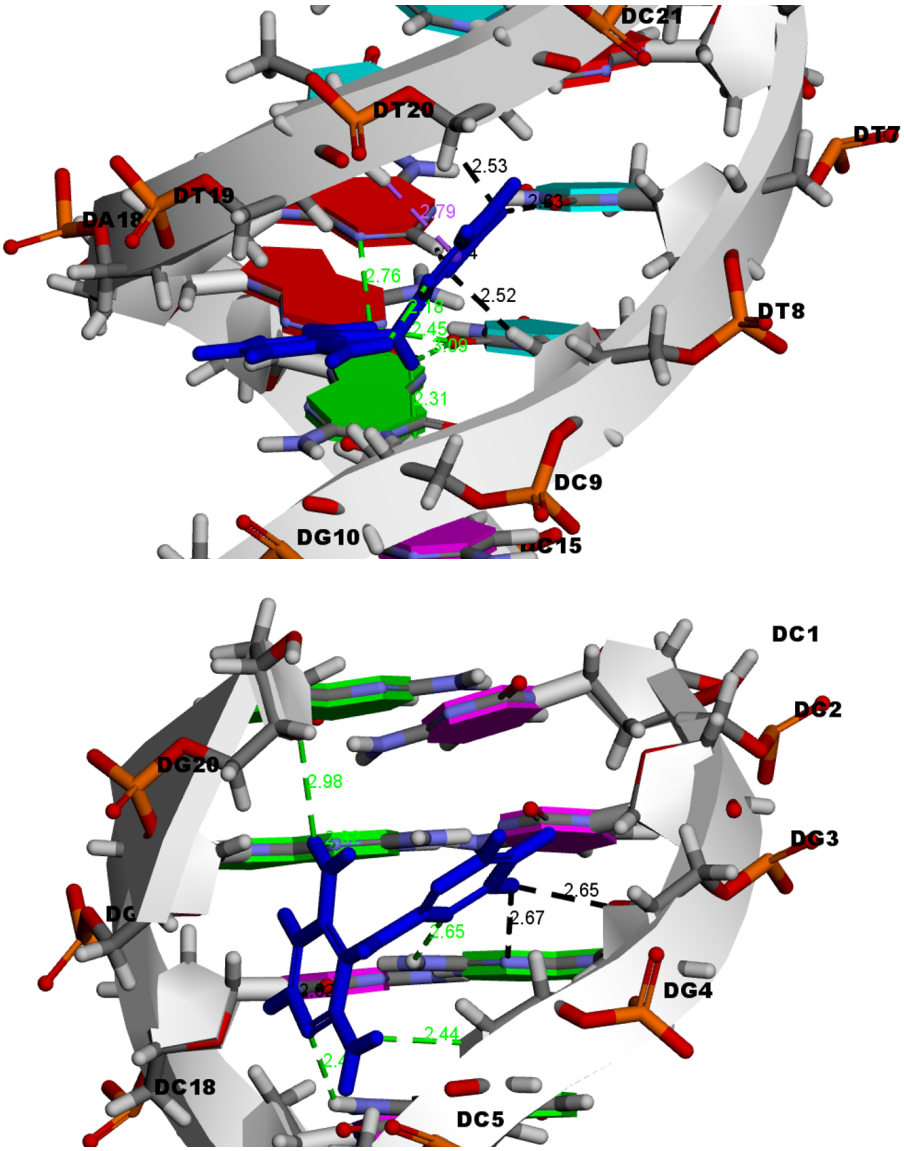

Figure 11. Molecular docked structures of **6** complexed with ctDNA models. Top: Represents the docked pose of **6** in the AT rich domain of minor groove of 1BNA model. B) Represents the docked pose in the CG rich region of minor groove of 1CGC model.